



Research Article

An experimental investigation of liquid jets under low-speed crossflows

Hatice MERCAN^{1,*}, Mehdi NABATI², Hasan BEDIR², Gunay ANLAS²

¹Department of Mechatronics Engineering, Faculty of Mechanical Engineering, Yildiz Technical University, İstanbul, 34349, Türkiye

²Department of Mechanical Engineering, Bogazici University, İstanbul, 34342, Türkiye

ARTICLE INFO

Article history

Received: 15 May 2024

Accepted: 11 August 2024

Keywords:

Droplet Formation; Gaseous Crossflow; Liquid Jet; Momentum Flux Ratio; Shadow Graph; Spray Penetration; Weber Number

ABSTRACT

This study presents the breakup mechanisms and droplet features of a liquid jet introduced into a low-speed cross air flow. The main aim of this study is to investigate the spray behavior of water when exposed to a uniform crossflow of air at very low velocities. A shadow sizing system is employed to collect comprehensive data for analyzing the interactions between liquid jets and crossflowing air. Three different nozzles were used to examine the distribution, penetration, and breakup characteristics of water jets in an air crossflow. It is worth highlighting that the Weber number in this experiment was maintained at a very low level. Both the jet Weber number ($1.3 < We_j < 119$) and the gas Weber number ($0 < We_g < 1$), along with the momentum flux ratio ($2 < q < 14400$), are crucial dimensionless parameters significantly affecting various droplet properties such as size, velocity, shape, and breakup behavior. This study investigates the structural features, trajectory of the jet, and duration of breakup near the nozzle. Subsequently, the experimental results are tabulated for future numerical and analytical studies. As the air crossflow velocity increases, the liquid jet bends in the direction of the airflow. The breakup length decreases with increasing air velocity. The nozzle with medium diameter shows the maximum dimensionless breakup length. At a constant air velocity, the breakup length initially increases and then decreases with an increasing momentum flux ratio. Higher liquid flow rates result in a higher density of smaller droplets. The liquid jets shift upstream with increasing q values; however, due to the wide range of q values, existing empirical relations in the literature fail to accurately predict this behavior.

Cite this article as: Mercan H, Nabati M, Bedir H, Anlas G. An experimental investigation of liquid jets under low-speed crossflows. J Ther Eng 2024;10(6):1411–1422.

INTRODUCTION

The physics of the complex behavior of the liquid jet in a cross air flow has been studied by many researchers. The interaction between the two flows is important for the overall effectiveness of the engineering applications like the lubrication of the air breathing engines [1],

or the flame stability and thus better energy conversion efficiency of the stationary and the avionic power generation systems [2, 3]. Thus it is essential to describe and better understand the droplet distribution, spray penetration and the break up mechanism of liquid jets in gaseous crossflow.

*Corresponding author.

*E-mail address: hmercan@yildiz.edu.tr

This paper was recommended for publication in revised form by Editor-in-Chief Ahmet Selim Dalkılıç



The basic stages of the breakup of the liquid jet under the influence of a crossflow are shown in Figure 1. The liquid column bends with the crossflow which forms ligaments due to capillary and column waves. The surface waves generate droplets that detach from the downwind surface of the liquid jet. Spray penetration represents the maximum distance traveled by the droplets in the transverse direction. The liquid column initially forms a set of ligaments, and at the end of the primary break up the first group of droplets is generated. The primary break up region and first generation droplets are mostly affected from the exit conditions at the nozzle [4]. The drop formation at different sizes is mostly observed at the secondary breakup region. The characteristics of the drops and the penetration of the jet column depend strongly on the crossflow regime [4], the liquid/gas flow momentum flux ratio and the injection angle [5].

Liquid jet in a cross air flow, studied extensively through experiments and numerical methods, present significant challenges. Experimental research encounters accuracy issues due to measurement techniques, complex operating conditions, and difficulty in observing near the injector nozzle [4]. Numerical methods encounter significant numerical challenges when dealing with high liquid-to-gas density ratios, viscosity ratios, and intense shear stresses at dynamic interfaces [6-8]. Studying liquid jets in cross air flows, whether through experimental or numerical means, is complicated due to the inherent complexity of the flow field. This difficulty is characterized by unsteady deformation and breaking of the interface. The wide range of temporal and spatial scales involved requires high resolutions, which pose challenges for both numerical simulations and experimental methods.

In this study, an experimental investigation is presented to understand the dynamics of liquid jet breakup,

atomization, and dispersion in a laminar cross air flow. Additionally, it aims to provide quantitative insights into liquid column penetration and the breakup mechanism. Section 2 provides a literature review focusing on liquid column penetration and break up mechanism. The problem outline and the considered parameters are listed as well. The experimental set up and calibrations are detailed in Section 3. Section 4 presents the results, discussing the physical mechanisms underlying liquid column atomization, while also detailing the penetration of the liquid column and the location of breakup. Finally, the droplet size distributions are provided.

The break up mechanism of a liquid jet in gaseous crossflow is generally investigated under different the crossflow regimes such as subsonic, supersonic and hypersonic [9-16]. Wu et al. [9] investigated the break up mechanism of three different liquid jets in a subsonic crossflow of air experimentally and reported a break up map as a function of the momentum flux ratio ($3.38 < q < 185$) and the gas Weber number ($57 < We_g < 594$). The multimode break up is reported where the liquid column break up arise into various bag shaped membranes at We_g around 60. As the We_g elevated, due to the accelerated waves, shear breakup of the droplets are observed. Tambe et al. [10] investigated experimentally the liquid jet break up mode for subsonic flows where $0.7 < q < 10.2$ and $50 < We_g < 1725$. At lower q and We_g , column break up is observed and for higher values of We_g or q a transitional zone of mixed mode took place followed by a surface break up mode. Singh et al. [14] reported the break up mechanisms and ligament distributions at supersonic crossflow where $4.19 < q < 8.43$. They subdivided the spray into four basic regions starting from the nozzle exit and identified the break up mechanisms using the average shear Weber number. They reported the critical shear Weber number equals to 80, where stripping ligament

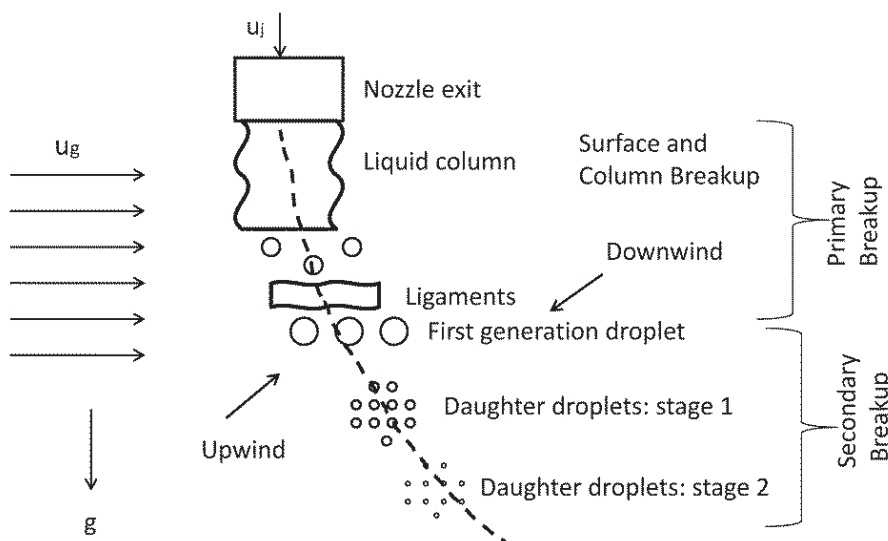


Figure 1. The schematic representation of the basic features of the liquid jet in a cross air flow.

mode is distinctive. Perurena et al. [16] investigated the jet break up for hypersonic air flow where $1.0 < q < 10.1$ with a uniform $Ma = 6$ crossflow. The shock fluctuations for liquid jet with $St = 0.18$ and for separation with $St = 0.011$ are reported. Stenzler et al. [17] investigated experimentally the liquid jet penetration in heated and unheated cross air flow. It is reported that the spray penetration is affected from We_g , μ , d and liquid column trajectory. Two correlations are presented for spray penetration as a function of q , We_g , μ for heated and unheated air conditions. They concluded that the spray penetration decreased with increasing We_g due to lower droplet diameters and increasing liquid viscosity increases the column bending due to enhanced drag.

The majority of the researches mentioned herein have examined the breakdown mechanisms of liquid jets that are introduced into a subsonic or supersonic air crossflow. These studies also include the measurement of sizes and velocities of droplets associated with the jet properties. In the context of the energy and chemical sector, it is common for gas velocity in industrial pipelines to range from 8-40 m/s [18]. The impact of aerodynamic force on the breakup of a liquid jet is rather limited, and the predominant mechanism of breakup for a liquid jet subjected to a low-speed crossflow differs significantly from that seen in the presence of a subsonic or supersonic crossflow. The suitability of breakdown properties and droplet distribution of liquid jets, for low-speed gas flow conditions has yet to be verified. In the literature, generally We_g and q are used to classify the break up regimes. Typically, the initial breakup of the liquid jet is classified into two primary modes: column breakup and surface breakup [9, 19, 20]. Column breakup refers to the splitting of the liquid column at a specified point, yielding large liquid fragments and droplet-like shapes. Similarly, surface breakup involves the shedding of liquid mass and detached structures along the column's path, resulting in smaller ligaments and droplets compared to column breakup. Primary breakup modes are described by various terms in the literature, such as column breakup, arcade-type breakup, or bag-like breakup [21]. The column breakup and the surface breakup are intrinsic to liquid jet gasoline combustion atomization, where one mode may dominate over the other based on the Weber number (We) and liquid flow rate [20]. Column breakup is further categorized into sub-regimes such as capillary/column breakup, bag breakup, multimode breakup, and shear breakup [9]. In certain conditions, when the nozzle diameter approaches or exceeds the liquid capillary length, another primary column breakup regime, known as multimode bag breakup, may occur [22].

For lower gas We , $We_g < 10$ the surface tension forces are larger than the aerodynamic forces. Aerodynamic forces bend the liquid jet, amplifying breakup due to capillary forces. This phenomenon is termed as enhanced capillary breakup, as illustrated by examples provided by Kitamura and Takahashi [23]. In a recent experimental study, Peters and Birouk [24] investigated the liquid jet breakup mechanism under the influence of the turbulence intensity of

the gas phase. The turbulence intensity affects the break up mechanism where multiple breakup regimes occur simultaneously. It is also reported that the break up length is lower for higher turbulence intensity and reaches a constant value beyond a significant momentum flux ratio. In the experimental study, Olyaei and Kebriaee [25] investigated the liquid sheet and jet in low-speed air crossflow. Their parameter range is $0.8 < We < 16.57$, $5 < q < 250$ and $380 < Re < 1850$. They compared six different nozzle shapes and reported column, bag and column-bag break up regimes for different nozzle geometries and cross section aspect ratio values. They reported rectangular nozzle geometry results more unstable jet with an earlier change of breakup characteristics compared to circular nozzles. Parakash et al. [26] investigated the effect of the nozzle exit size on liquid jets in air crossflow with parameter range of $17 < We < 89$ and $3 < q < 100$. They reported that the laminar jet has a greater ability to penetrate compared to the turbulent jet, resulting in a higher trajectory under comparable flow circumstances. The turbulent nature of the liquid jet leads to the liquid column breaking up sooner compared to the laminar jet due to its intrinsic instabilities. The liquid jet exhibits distinct forms of breakup at different frequencies. Although both the laminar and turbulent jets display similar motion, the turbulent jet is more intense, with greater amplitudes and shorter wavelengths for the corresponding modes. Zhang et al. [27] performed a numerical simulation using VOF technique to elucidate the break up regime of liquid jets in oscillating air crossflow. They reported when subjected to an oscillating flow, the back part of the jet starts to disintegrate sooner because the surface waves take longer to form. Over time, the velocity of the oscillating air input and the pace of surface wave creation both rise, eventually resulting in surface-wave-induced breakup. In oscillating crossflow, the penetration depth of the jet varies with the oscillating air velocity.

Accurate estimations of droplet size and velocity distributions are essential for assessing the atomization efficiency of the gas-liquid mixer, providing valuable feedback for design improvements and subsequent theoretical investigations. Understanding the atomization behavior of a liquid jet in a gaseous crossflow is crucial. The literature contains numerous studies exploring this phenomenon under both subsonic and supersonic airflow conditions, often accompanied by correlations relating to droplet size [18]. However there are very few works with slow cross air flow. The primary aim of this study is to elucidate the impact of momentum flux ratio and We_g on the break-up phenomena exhibited by liquid jets and the droplet distributions when subjected to a very low-velocity crossflow of air. The breakdown phenomena of liquid jets are captured using high-speed photography, while the droplet sizes and velocities are measured using shadow graph. The results could be applied in low-cost evaporative cooling systems, suitable for use in industrial and agricultural settings such as stock farming.

EXPERIMENTAL SETUP

The basic parameters that are essential to analyze the liquid jet in a gaseous crossflow can be categorized as the material properties of the liquid and the gas, the body forces, and the geometrical information inherited from the nozzle. The group of the parameters can be listed as the jet velocity (v_j), the gaseous crossflow velocity (u_g), the liquid and gas densities (ρ_l, ρ_g), the liquid and gas viscosities (μ_l, μ_g) and the surface tension (σ), the gravitational acceleration (g) and finally the tunnel hydraulic diameter (D_h), the jet diameter (d_j) and the tip angle (θ). The non-dimensional groups that are associated to jet flow in a gaseous cross are the momentum flux ratio, $q = \frac{\rho_l v_j^2}{\rho_g u_g^2}$, the jet and crossflow Reynolds numbers, Re_j, Re_g , the jet and the crossflow Weber number, $We_j = \frac{\rho_l v_j^2 d_j}{\sigma}, We_g = \frac{\rho_g u_g^2 d_j}{\sigma}$, and the density ratio of the two interacting fluids is $\frac{\rho_l}{\rho_g}$. The details of these parameters used in this study are listed in Table 1.

The experimental setup is located in BURET lab, Bogazici University. The tests were conducted in a blow down wind tunnel including a clear Plexiglas test section. The test section had a square cross section of 1m×1m and a length of 3.5m, as seen in Figure 2. The wind tunnel is outfitted with a centrifugal impeller that is powered by a 22kW motor. The motor is directly driven and has a Variable Frequency Drive (VFD) to regulate the air velocity inside the tunnel. The impeller diameter is 800 mm and is fitted with blades that have a rearward curved design. The zone of contraction may be described as a cubic arc, characterized by an area ratio of 6.25. To ensure the wind tunnel's calibration and minimize turbulence intensity, a dual screen mesh system is used. This system consists of two meshes, one coarse with a porosity of 65% and one fine with a porosity of 61%. Velocity measurements were

conducted at 16 equidistant locations along the vertical plane, situated 15 cm from the entrance of the test section. These measurements were carried out to assess the turbulence strength, with the specific position of the experiments being the focus of this research. The hot film anemometer is placed at the selected locations and a schematic representation of the selected locations is shown in Figure 3. An E+E Electronics, EE75 series airspeed transmitter is used to measure airspeed in the test section. The transmitter contains a hot film sensor that works on the thermal anemometric measuring principle. The sensor has two resistors placed on a glass sheet. The first resistor measures the temperature of the air flowing through the sensor (T_a), while the second resistor measures the heater temperature (T_h), where $T_h > T_a$. Due to the cooling effect of the blown air passing the sensor, the rate of temperature decrease can be related to the air velocity. The required electrical power (P) used to compensate for the cooling effect to keep the temperature difference $T_h - T_a$ constant is used as a measure for air velocity. Data were collected with IPETRONIK software and M-SENS-8 module. Appropriate data acquisition time and sampling rate are selected to maintain reliable velocity measurements. In the study conducted by Murzyn and Belogey for a turbulent flow, the measurement time was chosen as 50 s and the speed was chosen as 5000 Hz [28, 29]. In this study, a single experiment lasted 15 minutes and data collected in the last 5 minutes of each session was used for analysis. Therefore, for the results presented in this study, the data collection time was chosen as 300 s and the sampling rate was 1000 Hz. The data obtained from these measurements is gathered at a frequency of 1000 Hz for duration of 300 seconds. The tunnel's average turbulence intensity is guaranteed to be below 0.5% for all air speed values. The wind tunnel is capable of attaining a maximum air velocity of 8 m/s.



Figure 2. Blow down type low speed wind tunnel, the contraction cone and the transparent test section.

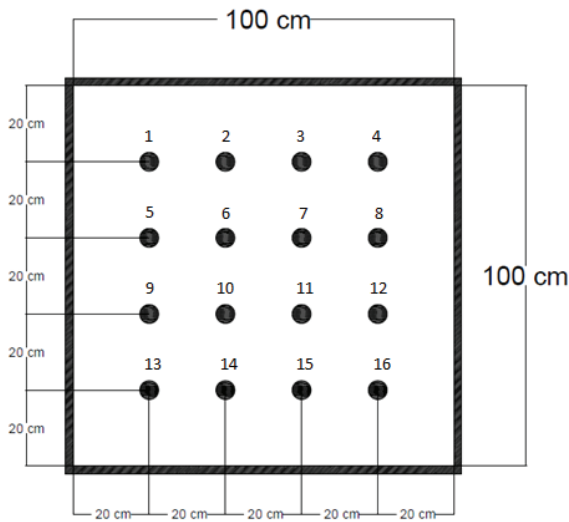


Figure 3. Speed measurement locations along the test section.

Table 1. The details of the geometric and material properties

Liquid jet velocity, v_j , ms^{-1}	0-0.13
Nozzle inner diameter, d_N , mm	0.514-0.603-1.194
Surface tension, σ , Nm^{-1}	0.0728
Air velocity, u_g , ms^{-1}	0-5
Liquid-gas momentum flux ratio, q	0-6000
Liquid density, ρ_l , kgm^{-3}	998.23
Liquid viscosity, μ , Pa.s	0.0010016
Air density, ρ_g , kgm^{-3}	2.422
Liquid Weber number, We_l	0-500
Gas Weber number, We_g	0-1

De-ionized water (DI) at room temperature and constant pressure is introduced into the test area by a ceiling-mounted nozzle placed at a distance of 15 cm from the entrance. Figure 4 shows the schematic of the experimental setup. The fluid is delivered using an injection system that maintains a consistent gauge pressure of 65 centimeters of water column. Three commercially available syringe needles of different diameters, namely 16G (N1), 20G (N2), and 21G (N3), are used as nozzles. The nozzles are positioned

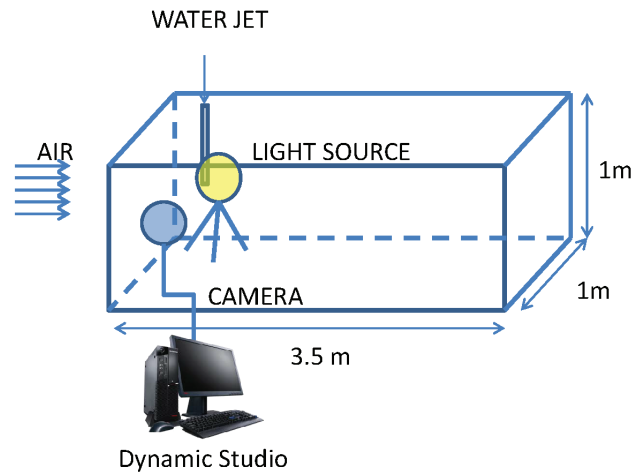


Figure 4. Schematic representation of the experimental setup.

inside the setup section ensuring that the course of the jet is not disrupted by the bevel section. Table 2 provides the test conditions and their corresponding ranges.

Flow Visualization

The experimental configuration comprises a Particle Imaging Velocity meter (PIV) equipped with twin cavity flash-pumped Nd:YAG lasers. The lasers have a repetition rate of 15 Hz, pulse energy of 135 mJ, and emit light at a wavelength of 532 nm. The PIV technique is used to conduct velocity vector measurements of the whole flow field.

Shadowgraph is a commonly used technique for quantifying the dimensions, morphology, and motion characteristics of droplets. The integration of the Shadow-Strobe and Dual-Power laser technologies provides a consistent and powerful background illumination that is free from speckles. Additionally, the use of an 8-megapixel CCD camera (FlowSense EO 8M) with a macro lens enables the capture of high-quality close-up photographs. The evaluation of cumulative histograms, histograms of size distribution, and spatial distribution plots of droplets is conducted via the analysis of photographs using the Dantec Dynamic Studio program.

A total of 100 photographs, each with a resolution of 1267×9546 pixels², are obtained to visualize the behavior of the water liquid jet in a cross air flow. A transparent ruler is used as a calibration target, and the shadow picture was adjusted in relation to this target. The measured scale factor is 1.579 for the specified distance of 10 millimeters. The

Table 2. Experimental conditions: nozzle inner diameter sizes, air crossflow speed and water jet volumetric flow rates

Nozzle Name	Nozzle Diameter ($\times 10^{-3}\text{m}$)	u_g (m/s)	\dot{Q}_j (ml/s)
N1	0.514	0-1-3-5	0.01-0.02-0.025
N2	0.603	0-1-3-5	0.01-0.02-0.025
N3	1.194	0-1-3-5	0.01-0.02-0.025

diameters of the droplets are acquired from the captured images, while the velocity of each droplet is determined by comparing two consecutive photos. This enables the calculation of the distance traveled by each droplet.

RESULTS AND DISCUSSION

The breakup of a liquid jet includes two consecutive phenomena, namely primary and secondary breakup. In the context of a cross airflow, as seen in Figure 1, the main fragmentation of a liquid jet is influenced by two distinct processes, namely column breakup and surface breakup. The disintegration of ligaments and droplets from a liquid column occurs via the primary breakup process. This is followed by a secondary breakup mechanism, which results in the development of smaller droplets. Ultimately, this leads to the generation of a spray in the far-field area. The subsequent sections will address the distinct characteristics of droplets and their production processes in the near-field and far-field regions of a low speed crossflow liquid jet. In this study the air flow is fully developed, uniform with low speed and turbulence intensity (less than 5% for all wind speeds) where $We_g < 1$. Additionally the Reynolds and the Weber numbers for the water jet are moderate which increased the momentum flux ratio significantly. For the best of authors knowledge, the cases with moderate jet velocities and low air speed with $We_g < 1$ is not addressed in the literature and this study aims to fill this gap and concentrate on the break up properties, droplet distributions and surface instabilities of liquid jets in a very low We crossflows. The experimental parameters with their corresponding non-dimensional groups are listed in Table 1 and Table 2 respectively.

The studies in the literature generally focused on investigation of liquid jets subjected to subsonic and supersonic crossflows. There are very few attempts for low air velocity cases where $We_g \sim 4$ [18]. In this study the analysis is focused on low gas Weber number in the range of $0 < We_g < 1$ which leads to considerably high momentum flux ratios. The low turbulence intensity is ensured in wind tunnel which resulted with droplet shapes to be almost spherical and only column break up regime is observed. Although some surface fluctuations are observed, no bag and bump break up regimes are observed and the mean diameter of the droplets are between $100 - 200 \mu m$, as reported in the literature [18, 30].

Effect of the Cross Air Velocity

The effect of increasing cross air velocity on the liquid column, droplet formation and distribution is investigated using the shadowgraph flow visualizations.

In Figure 5, the shadow sizer views are presented for the nozzle N1, at volumetric flow rate 0.02 ml/s, for increasing air velocities. In Figure 5a, the water jet is subjected to a quiescent air, $u_g = 0$ m/s where the liquid jet is almost straight and the droplets are not dispersed, as expected. In Figure 5b, the cross air velocity is $u_g = 1$ m/s, the liquid

jet still straight however the droplets are significantly dispersed and some daughter droplets are visible especially in the air flow direction. In Figure 5c, the air velocity is $u_g = 3$ m/s, the liquid jet is bent slightly in the vicinity of break up point but the droplet dispersion is significant and the droplets are located in the direction of the air flow. As the crossflow velocity increased to $u_g = 5$ m/s, as shown in Figure 5d, the liquid jet bent significantly and the penetration depth became more visible. The droplet dispersion is more pronounced and the droplets are located on a bent alignment in the air flow direction. The nozzle under consideration exhibits a smooth surface on both the upwind and downwind sides of the jet column, with no observable surface fluctuations. The first stage daughter droplets are formed however the second stage daughter droplets are sparsely distributed for the highest cross air velocity case. At higher crossflow velocities, the liquid jet column becomes curved in the direction of the airflow.

Figure 6 displays the shadow sizer views for nozzle N2 at a volumetric flow rate of 0.02 ml/s, demonstrating the progressive air velocities. In the instances of quiescent and $u_g = 1$ m/s, the penetration depth is seen to be zero. However, it is worth noting that the length of the liquid column is greater than that of the first nozzle N1, as shown in Figure 6a and 6b, respectively. Furthermore, the daughter droplets of the second stage become perceptible. With increasing velocity of air crossflow, both the liquid column and the droplets are deflected towards the direction of the air flow. Furthermore, the daughter droplets in the second stage exhibited increased density and dispersion along the direction of the airflow. Similar to the N1, the N2 nozzle demonstrates a consistent surface on both the upwind and downwind aspects of the jet column, devoid of any discernible surface fluctuations.

The shadowgraph images for nozzle N3 at a volumetric flow rate of 0.02 ml/s are shown in Figure 7, illustrating the gradual variations in air velocities. In cases when the flow is quiescent and the air velocity is equal to 1 m/s, it is observed that the penetration depth is found to be zero.

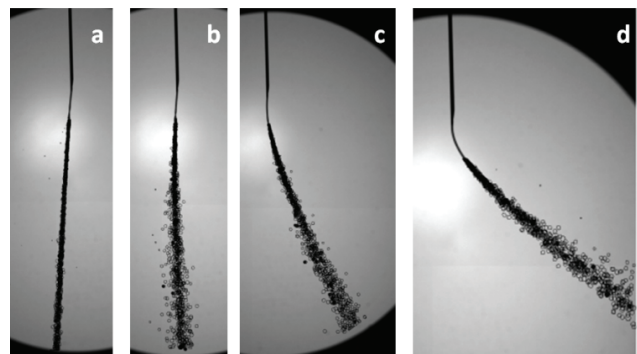


Figure 5. Effect of air crossflow velocity on the liquid column and droplet dispersion for nozzle N1, flow rate 0.02 ml/s. (a) $u_g = 0$ m/s, (b) $u_g = 1$ m/s, (c) $u_g = 3$ m/s, (d) $u_g = 5$ m/s.

It is important to acknowledge that the length of the liquid column is greater than that of the first nozzle N1, but shorter than nozzle N2, as seen in Figure 7a and 7b, respectively. The diameter of the N3 nozzle is the greatest, resulting in

a notable increase in the diameter of the daughter droplets. As the velocity of air crossflow increases, both the liquid column and the droplets experience deflection in the direction of the air flow. The N3 nozzle exhibits a uniform

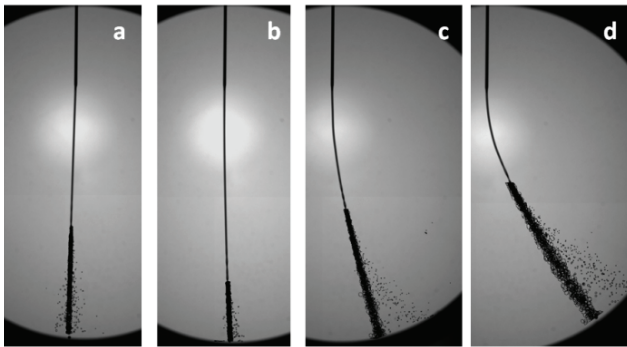


Figure 6. Effect of air crossflow velocity on the liquid column and droplet dispersion for nozzle N2, flow rate 0.02 ml/s. (a) $u_g = 0$ m/s, (b) $u_g = 1$ m/s, (c) $u_g = 3$ m/s, (d) $u_g = 5$ m/s.

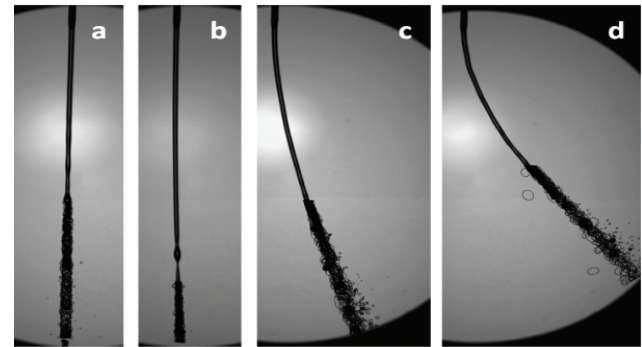
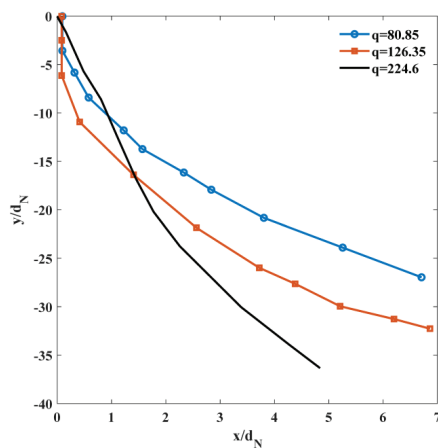
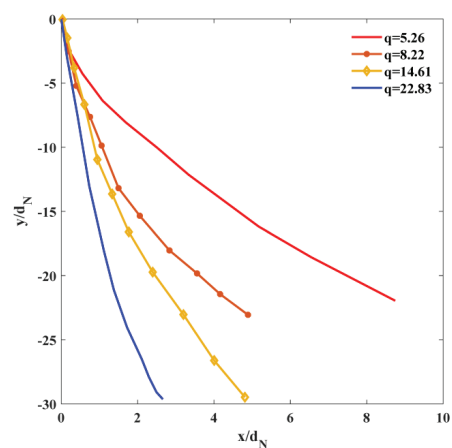


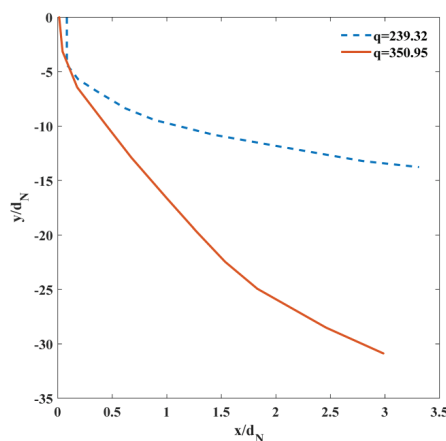
Figure 7. Effect of air crossflow velocity on the liquid column and droplet dispersion for nozzle N3, flow rate 0.02 ml/s. (a) $u_g = 0$ m/s, (b) $u_g = 1$ m/s, (c) $u_g = 3$ m/s, (d) $u_g = 5$ m/s.



(a)



(b)



(c)

Figure 8. Experimentally obtained dimensionless jet projection profiles for increasing momentum flux ratios (a) low, (b) medium, (c) high.

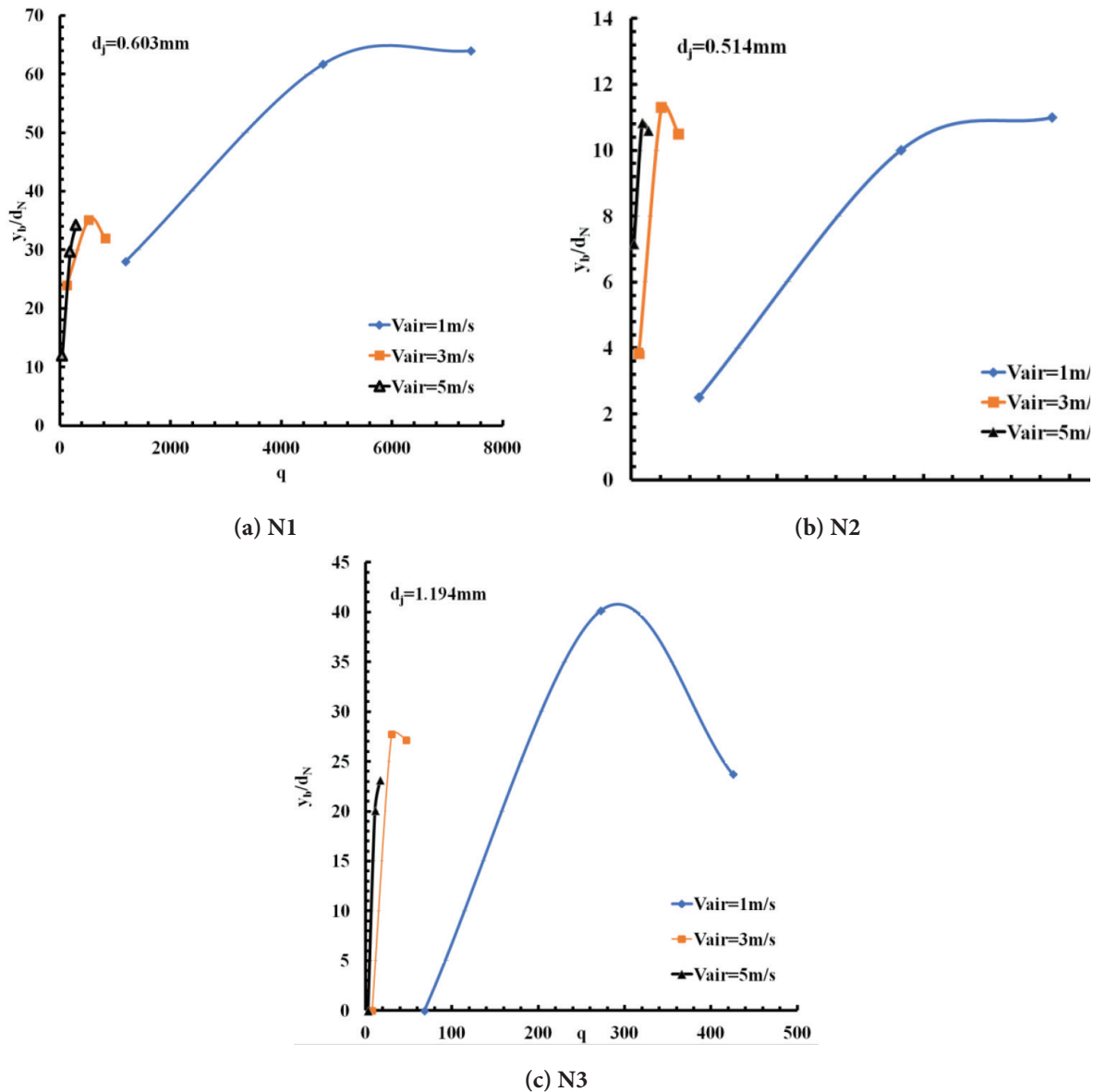


Figure 9. Effect of air crossflow velocity on the dimensionless breakup lengths for increasing momentum flux ratios for three different nozzle diameters. (a) N1 (b) N2, (c) N3.

surface on both the upwind and downwind sides of the jet column, without any noticeable surface irregularities, much like the nozzles, N1 and N2.

The available empirical relations for the jet projection is defined generally as a function of momentum flux ratio only and some of them are defined by introducing the jet Reynolds number to the relation. However they are proposed for considerably low q values where especially gas Weber number is significant. In Figure 8a, b and c the experimentally obtained liquid jet projections are shown for increasing q values at three categories, low, medium and large q values, respectively. It is observed that the liquid jets moved in the upstream direction with increasing q values, similar to the observations in the literature [4]. Available

empirical relationships do not accurately predict the experimentally obtained liquid jet profiles as a result of the wide range of q values.

The variation of dimensionless breakup length with increasing air velocities for each of the three nozzles is summarized in Figure 9. Although the momentum flux ratio is high at low air velocities, the breakup length increases as the air velocity decreases. Similar results are reported by Peters and Birouk in the literature with higher turbulence intensity [30]. In the second nozzle, Figure 9b, the dimensionless breakup length exceeds 60. In the third nozzle, Figure 9c, the increase in momentum flux has even decreased the breakup length at low air velocities. Alternatively, Figure 10 displays the changes in dimensionless breakup length

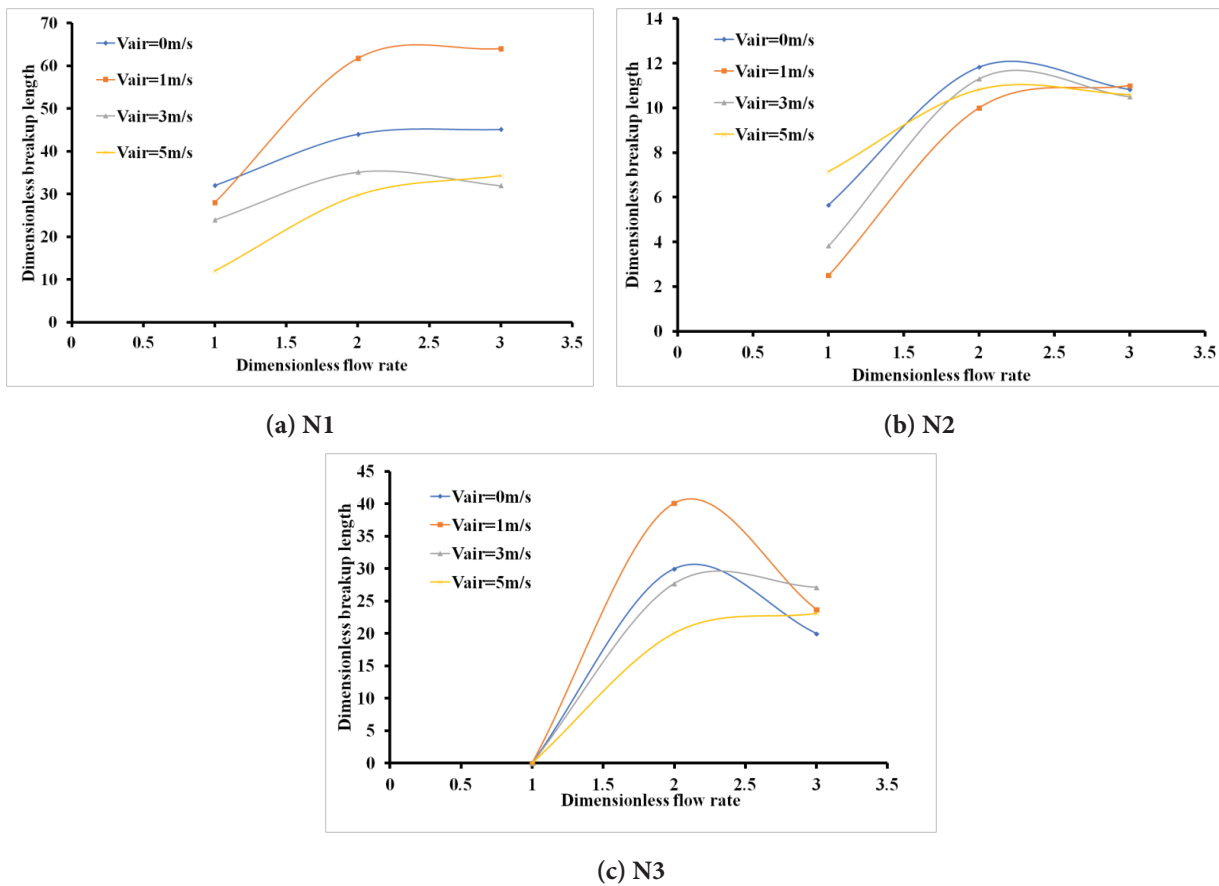


Figure 10. Effect of air crossflow velocity on the dimensionless breakup lengths for increasing flow rates for three different nozzle diameters. (a) N1 (b) N2, (c) N3.

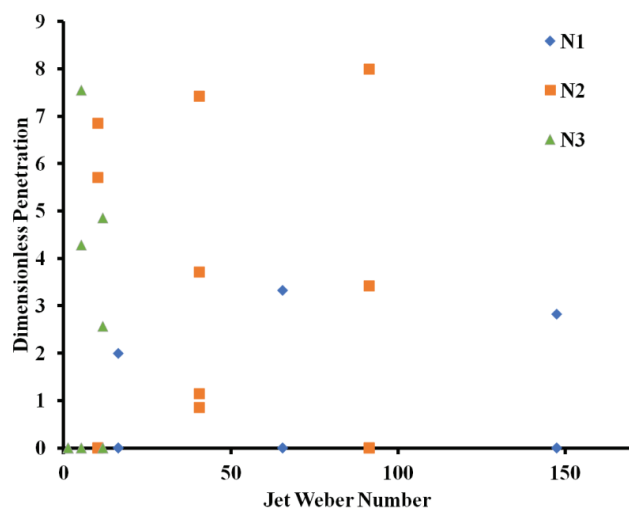


Figure 11. Effect of jet Weber number on the dimensionless penetration depth for three different nozzle diameters.

across three different nozzles as air velocity increases with varying flow rates. For all nozzles, an increase in flow rate resulted in a longer breakup length at low and medium flow rates. In nozzle 1, further increases in flow rate led to

a slight decrease in breakup length (Figure 10a). For nozzle 2 (Figure 10b), a further increase in flow rate caused the breakup length to plateau. In nozzle 3 (Figure 10c), the highest flow rate resulted in a sharp decrease in breakup length, indicating earlier droplet formation. Additionally, the breakup length is longest in nozzle 2 and shortest in nozzle 1.

For a liquid jet introduced into a crossflow, penetration depth indicates the distance the jet can travel into the airflow before it mixes substantially with the surrounding air and loses its distinct profile. In this study, the penetration depth is scaled by the nozzle diameter to become dimensionless. Figure 11 illustrates the dimensionless penetration depth for varying nozzle diameters and Jet Weber numbers. For nozzle 1, the penetration depth is zero at both low and medium air velocities. In contrast, nozzles 2 and 3 exhibited greater penetration depths at higher air velocities.

Finally the droplet size distribution along the sample is determined and the statistical distributions are shown in Figure 12. The measured points are almost in the form of normal distribution, similar to the observations of Kong et al. [18]. In Figure 12, the droplet size distribution along the jet is shown for N1, at maximum crossflow velocity, 5m/s

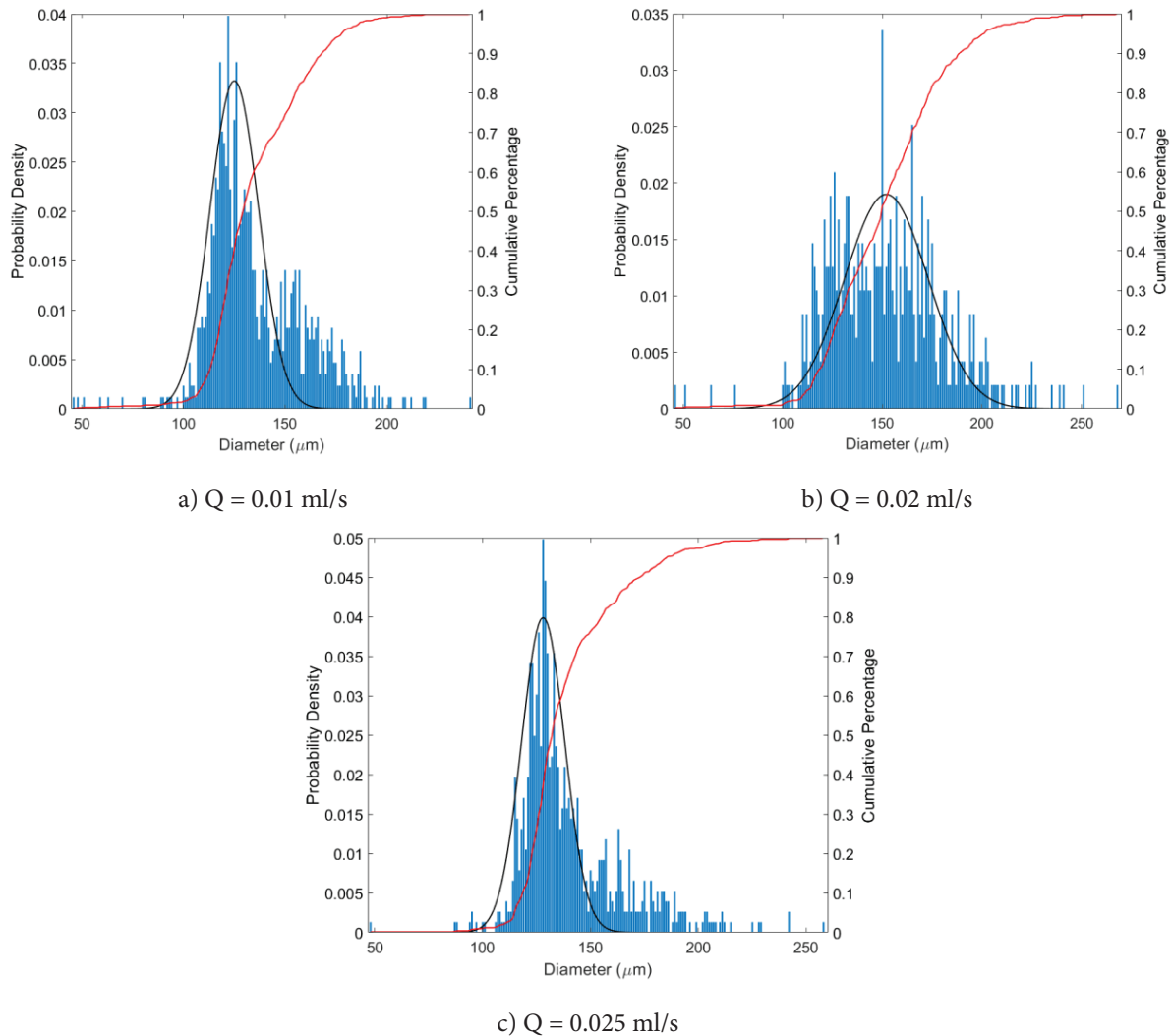


Figure 12. Effect of flow rate on the droplet size for nozzle N2, $V_{air} = 5 \text{ ml/s}$, (a) $Q = 0.01 \text{ ml/s}$ (b) $Q = 0.02 \text{ ml/s}$, (c) $Q = 0.025 \text{ ml/s}$.

and for increasing flow rates. The mean droplet diameter decreased with increasing flow rate. The distribution is thicker and lower for low rates and for increasing flow rates they are thinner and higher. The droplet size distribution shows two distinctive peaks for all flow rate regimes. For flow rate 0.01, the probability of small and large droplets is almost the same, however as the flow rate increase the smaller size droplets (daughter) are more common compared to larger droplets.

The studies in the literature generally focused on investigation of liquid jets subjected to subsonic and supersonic crossflows. There are very few attempts for low air velocity cases where $We_g \sim 4$ [18]. In this study the analysis is focused on low gas Weber number in the range of $0 < We_g < 1$ which leads to considerably high momentum flux ratios. The low turbulence intensity is ensured in wind tunnel which resulted with droplet shapes to be almost spherical and only column break up regime is observed. Although some surface fluctuations are observed, no bag and bump break up regimes are

observed and the mean diameter of the droplets are between $100 - 200 \mu\text{m}$, as reported in the literature [18, 30].

CONCLUSION

Most literature studies focus on liquid jets in subsonic and supersonic crossflows, with few addressing low air velocity cases where $We_g \sim 4$. This study examines low gas Weber numbers ($0 < We_g < 1$), resulting in high momentum flux ratios. Low turbulence intensity in the wind tunnel ensured nearly spherical droplet shapes, with only column breakup observed. Despite some surface fluctuations, no bag or bump breakup regimes occurred, and droplet diameters ranged between $100\text{-}200 \mu\text{m}$.

In this study the liquid jet in a laminar air crossflow is studied experimentally. Three different nozzles with 4 different air velocities are subjected to three different liquid flow rates are investigated. The conclusions can be summarized as the following:

- For increasing air crossflow velocity, the liquid jet bends towards the air velocity.
- For increasing air flow velocity the breakup length decreased. The maximum dimensionless breakup length is observed in nozzle N2.
- At constant air velocity, the increase in momentum flux ratio first increased then decreased the breakup length.
- At small and medium flow rates, the breakup length increased; however, at higher flow rates, it either reached a plateau or resulted in earlier breakup.
- The dimensionless penetration depth increased with air velocity.
- The smaller size droplet density is enhanced with increasing liquid flow rate.
- The liquid jets moved towards the upstream direction with increasing q , however due to wide range of q values the empirical relations in the literature failed to predict them accurately.

The low-speed crossflow of liquid jets shows promise for use in evaporative cooling systems with low maintenance costs. In these systems, droplet atomization significantly enhances evaporation. Further investigation is needed to understand the relationship between nozzle geometry, the breakup mechanism, and evaporation.

NOMENCLATURE

d	diameter
D	hydraulic diameter
DI	De-ionized water
g	gravitational acceleration
u	air velocity
v	jet velocity
PIV	Particle Imaging Velocity meter
q	momentum flux ratio
Q	volumetric flow rate
Re	Reynolds Number
St	Strouhal number
T	temperature
VFD	Variable Frequency Drive
We	Weber Number

Greek symbols

μ	viscosity
ρ	density
σ	surface tension
θ	tip angle

Subscripts

a	air
g	gas
h	heater
j	jet
N	nozzle

ACKNOWLEDGMENT

This work was supported by a grant of the Yildiz Technical University Scientific Research Project Coordination Unit, YTU-BAPK, Project no: FBA-2018-3421.

AUTHORSHIP CONTRIBUTIONS

Authors equally contributed to this work.

DATA AVAILABILITY STATEMENT

The authors confirm that the data that supports the findings of this study are available within the article. Raw data that support the finding of this study are available from the corresponding author, upon reasonable request.

CONFLICT OF INTEREST

The author declared no potential conflicts of interest with respect to the research, authorship, and/or publication of this article.

ETHICS

There are no ethical issues with the publication of this manuscript.

REFERENCES

- [1] Birouk M, Stähler T, Azzopardi BJ. An experimental study of liquid jets interacting with cross airflows. *Part Part Syst Charact* 2003;20:39–46. [\[CrossRef\]](#)
- [2] Karagozian AR. Transverse jets and their control. *Prog Energy Combustion Sci* 2010;36:531–553. [\[CrossRef\]](#)
- [3] Desantes JM, Arrègle J, López JJ, García JM. Turbulent gas jets and diesel-like sprays in a crossflow: A study on axis deflection and air entrainment. *Fuel* 2006;85:2120–2132. [\[CrossRef\]](#)
- [4] Broumand M, Birouk M. Liquid jet in a subsonic gaseous crossflow: Recent progress and remaining challenges. *Prog Energy Combustion Sci* 2016;57:1–29. [\[CrossRef\]](#)
- [5] Kasmaiee S, Tadjfar M. Influence of injection angle on liquid jet in crossflow. *Int J Multiphase Flow* 2022;153:104128. [\[CrossRef\]](#)
- [6] Pai M, Bermejo-Moreno I, Desjardins O, Pitsch H. Parametric study of primary breakup of turbulent liquid jets in crossflow: Role of Weber number. 48th AIAA Aerospace Sciences Meeting Including the New Horizons Forum and Aerospace Exposition, Orlando, Florida; 4-7 Jan 2010. p. 212. [\[CrossRef\]](#)
- [7] Prakash SR, Jain SS, Lovett JA, Raghunandan BN, Ravikrishna RV, Tomar G. Detailed numerical simulations of atomization of a liquid jet in a swirling gas crossflow. *Atom Sprays*, 2019;29:577–603. [\[CrossRef\]](#)

- [8] Mukundan AA, Tretola G, Ménard T, Herrmann M, Navarro-Martinez S, Vogiatzaki K, et al. DNS and LES of primary atomization of turbulent liquid jet injection into a gaseous crossflow environment. *Proc Combust Inst* 2021;38:3233–3241. [\[CrossRef\]](#)
- [9] Wu PK, Kirkendall KA, Fuller RP, Gruber MR, Nejad AS. Spray trajectories of liquid fuel jets in subsonic crossflows. *Int J Fluid Mech Res* 1997;24:128–137. [\[CrossRef\]](#)
- [10] Tambe S, Jeng SM, Mongia H, Hsiao G. Liquid jets in subsonic crossflow. 43rd AIAA Aerospace Sciences Meeting and Exhibit, Reno, Nevada; 11 Jan 2005. p. 731. [\[CrossRef\]](#)
- [11] Yoo YL, Han DH, Hong JS, Sung HG. A large eddy simulation of the breakup and atomization of a liquid jet into a cross turbulent flow at various spray conditions. *Int J Heat Mass Transf* 2017;112:97–112. [\[CrossRef\]](#)
- [12] Schetz JA, Kush EA Jr, Joshi PB. Wave phenomena in liquid jet breakup in a supersonic crossflow. *AIAA* 1980;18:774–778. [\[CrossRef\]](#)
- [13] Wu L, Wang ZG, Li Q, Zhang J. Investigations on the droplet distributions in the atomization of kerosene jets in supersonic crossflows. *Appl Physics Letters* 2015;107:104103. [\[CrossRef\]](#)
- [14] Singh V, Joseph NC, Thakor N, Chaudhuri S. Liquid Jet Interaction with Supersonic Crossflow. *AIAA Scitech 2020 Forum*, Orlando, FL; 6-10 Jan 2020. p. 1613. [\[CrossRef\]](#)
- [15] Catton I, Hill DE, McRae RP. Study of liquid jet penetration in a hypersonic stream. *AIAA* 1968;6:2084–2089. [\[CrossRef\]](#)
- [16] Perurena JB, Asma CO, Theunissen R, Chazot O. Experimental investigation of liquid jet injection into Mach 6 hypersonic crossflow. *Experiments Fluids* 2009;46:403–417. [\[CrossRef\]](#)
- [17] Stenzler JN, Lee JG, Santavicca DA, Lee W. Penetration of liquid jets in a cross-flow. *Atom Sprays* 2006;16:887–906. [\[CrossRef\]](#)
- [18] Kong L, Lan T, Chen J, Wang K, Sun H. Breakup processes and droplet characteristics of liquid jets injected into low-speed air crossflow. *Processes* 2020;8:676. [\[CrossRef\]](#)
- [19] Mazallon J, Dai Z, Faeth GM. Primary breakup of nonturbulent round liquid jets in gas crossflows. *Atom Sprays* 1999;9:291–311. [\[CrossRef\]](#)
- [20] Madabhushi RK, Leong MY, Arienti M, Brown CT, McDonell VG. On the breakup regime map of liquid jet in crossflow. *ILASS Americas, 19th Annual Conference on Liquid Atomization and Spray Systems*, Toronto, Canada; 2006.
- [21] Vich G, Ledoux M. Investigation of a liquid jet in a subsonic cross-flow. *Int J Fluid Mech Res* 1997;24:1–12. [\[CrossRef\]](#)
- [22] Scharfman B, Techet A, Bush J. Hydrodynamic instabilities in round liquid jets in gaseous crossflow. *APS Div Fluid Dynamics Meet Abst* 2011;64:R25–005.
- [23] Kitamura Y, Takahashi T. Stability of a liquid jet in air flow normal to the jet axis. *J Chem Engineer Japan* 1976;9:282–286. [\[CrossRef\]](#)
- [24] Peters J, Birouk M. Liquid jet breakup in a subsonic cross airflow: An experimental study of the effect of the gas phase turbulence. *Exp Comput Multiphase Flow* 2024;6:41–58. [\[CrossRef\]](#)
- [25] Olyaei G, Kebriaee A. Experimental study of liquid jets injected in crossflow. *Exp Therm Fluid Sci* 2020;115:110049. [\[CrossRef\]](#)
- [26] Prakash RS, Sinha A, Tomar G, Ravikrishna RV. Liquid jet in crossflow-effect of liquid entry conditions. *Exp Therm Fluid Sci* 2018;93:45–56. [\[CrossRef\]](#)
- [27] Zhang T, Song X, Kai X, He Y, Li R. Numerical simulation on primary breakup characteristics of liquid jet in oscillation crossflow. *Aero space* 2023;10:991. [\[CrossRef\]](#)
- [28] Manshadi MD. A new approach for turbulence reduction in a subsonic wind tunnel. PhD Thesis; Tehran, Iran: Sharif University of Technology; 2009.
- [29] Manshadi MD. The importance of turbulence reduction in assessment of wind tunnel flow quality. In: Lerner JC, Boldes U, eds. *Wind Tunnels and Experimental Fluid Dynamics Research*. InTech; 2011.
- [30] Lubarsky E, Reichel JR, Zinn BT, McAmis R. Spray in crossflow: Dependence on Weber number. *J Engineer Gas Turbines Power* 2009;132:021501. [\[CrossRef\]](#)